# *In situ* X-ray absorption spectroscopic studies of TiO$_2$ photocatalytic active sites for degradation of trace CHCl$_3$ in drinking water

**T.-L. Hsiung,[a] L.-W. Wei,[a] H.-L. Huang[b] and H. Paul Wang[a]\***

[a]Department of Environmental Engineering, National Cheng Kung University, Tainan, 70101, Taiwan, and [b]Department of Safety, Health and Environmental Engineering, National United University, Miaoli 36063, Taiwan.
*Correspondence e-mail: wanghp@ncku.edu.tw

Edited by R. W. Strange, University of Essex, United Kingdom

Toxic disinfection byproducts such as trihalomethanes (*e.g.* CHCl$_3$) are often found after chlorination of drinking water. It has been found that photocatalytic degradation of trace CHCl$_3$ in drinking water generally lacks an expected relationship with the crystalline phase, band-gap energy or the particle sizes of the TiO$_2$-based photocatalysts used such as nano TiO$_2$ on SBA-15 (Santa Barbara amorphous-15), TiO$_2$ clusters (TiO$_2$–SiO$_2$) and atomic dispersed Ti [Ti-MCM-41 (Mobil Composition of Matter)]. To engineer capable TiO$_2$ photocatalysts, a better understanding of their photoactive sites is of great importance and interest. Using *in situ* X-ray absorption near-edge structure (XANES) spectroscopy, the A$_1$ (4969 eV), A$_2$ (4971 eV) and A$_3$ (4972 eV) sites in TiO$_2$ can be distinguished as four-, five- and six- coordinated Ti species, respectively. Notably, the A$_2$ Ti sites that are the main photocatalytic species of TiO$_2$ are shown to be accountable for about 95% of the photocatalytic degradation of trace CHCl$_3$ in drinking water (7.2 p.p.m. CHCl$_3$ gTiO$_2^{-1}$ h$^{-1}$). This work reveals that the A$_2$ Ti species of a TiO$_2$-based photocatalyst are mainly responsible for the photocatalytic reactivity, especially in photocatalytic degradation of CHCl$_3$ in drinking water.

## 1. Introduction

In order to decrease the risk of water-borne diseases, chlorine is used in the disinfection of drinking water. However, toxic disinfection byproducts (DBPs) such as trihalomethanes (THMs) are frequently formed in the drinking water chlorination processes. The US National Cancer Institute has suggested that chloroform (one of the THMs) is carcinogenic in rodents (Boorman, 1999). Lin & Hoang (2000) found that the level of THM carcinogen exposure could be as high as 47 µg day$^{-1}$ by drinking or 30 µg day$^{-1}$ by inhalation. Conventional methods for reduction of DBPs and precursors include chemical coagulation, activated carbon adsorption, membrane separation, ozonation and combined ozonation/ bio-treatments (Pan *et al.*, 2016; Sillanpää *et al.*, 2018; Cai *et al.*, 2018; Abou-Gamra & Ahmed, 2015). Membrane separation and ozonation also are highly efficient in the reduction of biologically unstable materials. However, those methods may not be economically attractive in engineering applications (Sillanpää *et al.*, 2018; Cai *et al.*, 2018).

TiO$_2$, which possesses unique characteristics such as high photostability, effective band gap and easy availability, has been widely applied in the photocatalytic degradation of toxic organics, splitting of H$_2$O, reduction of NO to N$_2$, and dye-sensitized solar cells (Guo *et al.*, 2018; Kang & Wang, 2013; Yang *et al.*, 2014; Xie *et al.*, 2017; Liao *et al.*, 2014). The photocatalytic activities of TiO$_2$ can be enhanced with
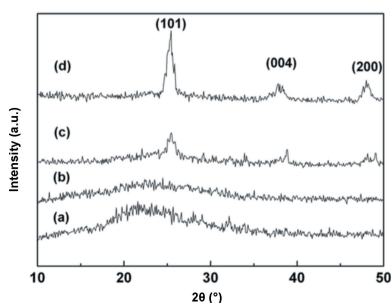
dispersed transition metal promoters such as V, Cr, Fe, Cu, Ni, Mn, Ag or Au (Yang *et al.*, 2017; Wang *et al.*, 2017; Lin *et al.*, 2017; Muñoz-Batista *et al.*, 2014). Nano $TiO_2$ has been considered a desirable photocatalyst due to its large surface-to-volume ratios (Xu *et al.*, 2019; Chen *et al.*, 2019).

Valence and local structure (<1 nm) of select elements in a complicated solid matrix can be studied by synchrotron X-ray absorption spectroscopy. Molecular structure information such as the coordination number (CN), bond distance and oxidation state of elements can be determined by X-ray absorption [extended X-ray absorption fine structure (EXAFS) and X-ray absorption near-edge structure (XANES)] spectroscopy. Using XANES and EXAFS, it was found that copper oxide clusters in the channels of mesopores (2–6.5 nm) [MCM-41 (Mobil Composition of Matter-41)], micropores (0.54–0.56 nm) [*e.g.* ZSM-5 (Zeolite Socony Mobil-5) and ZSM-48] and $TiO_2$-based photocatalysts were very effective in catalysis (Hsiung *et al.*, 2006a, 2021; Chien *et al.*, 2001; Huang *et al.*, 2003). These molecular-scale data turn out to be very useful in revealing the nature of catalytic active species and the reaction paths involved.

Photocatalytic degradation of trace THMs or DBPs by nano $TiO_2$ was shown to be not very effective (Diaz-Angulo *et al.*, 2019; El-Mragui *et al.*, 2019). On the other hand, photo-catalytic generation of $H_2$ (from $H_2O$) on atomic dispersed Ti and Zr in the mesoporous molecular sieve (MCM-41) (Ti-MCM-41 and Zr-MCM-41) can be enhanced by 17 and 80 times, respectively (if compared with the bulk states) (Liu *et al.*, 2003). It seems that nano, cluster (<4 nm in diameter) or even atomic dispersed $TiO_2$ may lead to unique enhancements in photocatalytic reactions. However, speciation of photo-catalytic active sites in $TiO_2$ has not been well studied parti-cularly during reactions (Hsiung *et al.*, 2006b, 2008). In order to prepare effective $TiO_2$ photocatalysts, a molecular-scale understanding of their photoactive sites is essential. Thus, the main objective of the present work was to study the chemical structure of Ti species with different $TiO_2$ sizes (*i.e.* nano, cluster and atomic dispersion) in relation to the photocatalytic degradation of trace $CHCl_3$ in drinking water by *in situ* XANES and EXAFS.

## 2. Experimental

The nano $TiO_2$–$SiO_2$ (Ti/Si atomic ratio = 3/7) photocatalyst was prepared by the sol-gel method (Beck *et al.*, 2001). Typi-cally, 12.8 g of titanium (IV) *n*-butoxide (Acros, 99%) and 24.3 g of tetraethylorthosilicate ($C_8H_{20}OSi$, TEOS) (Merck) were well mixed (at the pH value of 7.0) in an ethanol and distilled water (1:2) solution (45 ml). The $TiO_2$–$SiO_2$ solution was heated slowly until the sol-gel became xerogel, and then separated and calcined at 673 K for 1 h. The nano $TiO_2$ photocatalysts were synthesized using a similar procedure.

The $TiO_2$ supported on SBA-15 (Santa Barbara amorphous-15), that has a 2D hexagonal mesoporous structure with long straight channels parallel to the silica skeletons, photo-catalysts were prepared by co-condensation of silica, titanium oxide and neutral-charge poly(ethylene oxide)-poly(propyl-ene oxide)-poly(ethylene oxide) [$EO_{20}PO_{70}EO_{20}$ (P123)] (Aldrich, 99%) nonionic surfactant. Briefly, 0.21 g of titanium *n*-butoxide [Ti(OBu)$_4$, Aldrich, 97%] and 15 g of sulfuric acid (1.2 *M*, Merck) were well mixed until the solution became clear; a solution containing 2.75 g of sodium silica [14% NaOH and 27% $SiO_2$ (Aldrich)], 1.25 g of P123 (Aldrich, 99%) and 200 g of distilled water was added. The pH value of the solution was adjusted to 5.0. After separation, the photo-catalyst was calcined at 773 K for 6 h.

The Ti-inserted (framework) MCM-41 (Ti-MCM-41) photocatalysts were synthesized by the liquid crystal templating method. Fumed silica (Sigma) and sodium silicate solution were used as silica sources for the preparation of MCM-41. Hexadecyltrimethyl ammonium bromide (CTAB) (Sigma, purity >99%) and tetramethyl ammonium hydroxide [TMAOH, 25% (Sigma–Aldrich)] were used as a template and mineralizer, respectively. The mole ratio of $H_2O$, CTAB, TMAOH and Si in the mixture was 86:0.27:0.58:1. Titanium *n*-butoxide (Acros, 99%) was added to the MCM-41 mother liquid for the synthesis of Ti-MCM-41. A diluted sulfuric acid solution was used to adjust the pH values of the solution to between 11 and 12. The mixture was then heated in a Teflon-lined autoclave at 375 K for 24 h. The as-synthesized MCM-41 was filtered, washed with distilled water, dried and calcined at 773 K for 5 h.

The chemical structure of the photocatalysts was char-acterized by X-ray powder diffraction (XRD) spectroscopy (D8 Advance, Bruker) with Cu $K\alpha$ (1.542 Å) radiation. Samples were scanned from 10 to 50° ($2\theta$) at a scan rate of $5°$ min$^{-1}$. Diffuse reflectance ultraviolet/visible spectra (DR UV–vis) of the photocatalysts were also determined (between 200 and 700 nm) on a UV–vis spectrophotometer (Hitachi U-3010) at a scan speed of 120 nm min$^{-1}$.

The *in situ* Ti *K*-edge (4966 eV) XANES spectra of the photocatalysts were collected at 298 K on the wiggler beam-line of the Taiwan National Synchrotron Radiation Research Center. The absorption spectra were collected in ion chambers that were filled with helium and nitrogen mixed gases. The beam energy was calibrated to the adsorption edge of a Ti foil at the energy of 4966 eV. The electron storage ring was operated at an energy of 1.5 GeV (ring current = 120–200 A). The isolated EXAFS data were normalized to the edge jump and converted to the wavenumber scale. Fitting of data to model compounds was performed using *FEFFIT* (*UWXAFS 3.0*) in combination with the multiple scattering code *FEFF 8.0* simulation programs (Chiu *et al.*, 2011). *FEFFIT* was used to determine the best-fitting results with the minimum Debye–Waller factors (<0.01 Å$^2$). The Fourier transform was performed on $k^3$-weighted EXAFS oscillations in the range 3.8–11.7 Å$^{-1}$.

Photocatalytic degradation of $CHCl_3$ (500 p.p.b.) was performed on a homemade *in situ* EXAFS cell (Kang & Wang, 2013). Typically, 0.15 g of the $TiO_2$ photocatalyst was suspended in $H_2O$ containing trace $CHCl_3$ (500 p.p.b.). A 300 W high-pressure Xe arc lamp (Newport, model 6258) was used as the light source (250–800 nm) while the synchrotron X-ray absorption spectra of the $TiO_2$ photocatalysts were

determined. Concentrations of $CHCl_3$ were determined using a gas chromatograph (model 3400, Varian) equipped with an electrolytic conductivity detector (model 100, Tracor) and a purge/trap system (model LCS-2000, Tekmar).

## 3. Results and discussion

The XRD patterns of the $TiO_2$-based photocatalysts are shown in Fig. 1. The Ti-MCM-41 and $TiO_2$–$SiO_2$ photocatalysts have broadened peaks between 17 and 31° ($2\theta$), suggesting the absence of crystalline $TiO_2$, which may be associated with the existence of very small $TiO_2$ nanoparticles or highly atomic dispersed Ti therein. For the $TiO_2$/SBA-15 and nano $TiO_2$, anatase phases [(101), (004) and (200)] are observed with crystalline sizes of about 4.6 and 8.5 nm, respectively (calculated using the Scherrer equation).

Fig. 2 shows the DR UV–vis spectra of the photocatalysts. The band-gap energies for the $TiO_2$–$SiO_2$ and Ti-MCM-41 are 3.38 and 3.42 eV, respectively. Beck *et al.* (2001) also found blue shifts for the band-gap absorption edge with highly dispersed Ti in the $SiO_2$ framework. The absorption feature (<260 nm) for the Ti-MCM-41 can be attributed to the ligand-to-metal charge transfer between $Ti^{IV}$ and the amorphous $SiO_2$ framework. It seems that Ti is well dispersed in the Ti-MCM-41 photocatalyst.

The EXAFS spectra best-fitted by the Fourier transformation and $k^3$-weighted for the $TiO_2$-based photocatalysts in the ranges 0–4 and 4–11 Å, respectively, are shown in Fig. 3. The speciation parameters for the Ti in those photocatalysts are also listed in Table 1. The bond distances for the Ti—(O)—Si species (in the second shells) in the Ti-MCM-41 and $TiO_2$–$SiO_2$ photocatalysts are 3.13 and 3.31 Å, respectively. It is worth noting that the Ti-MCM-41 has a greater CN for the Ti—(O)—Si bonding than does the $TiO_2$–$SiO_2$, demonstrating that more Ti atoms are dispersed in the amorphous $SiO_2$ framework for the Ti-MCM-41, and that the $TiO_2$–$SiO_2$ one has more $TiO_2$ aggregates on the $SiO_2$ surfaces with a metal–
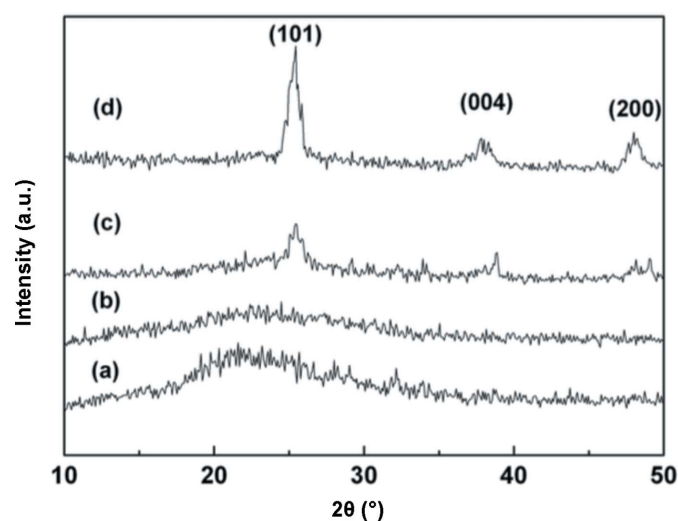
**Table 1**
Speciation parameters of titanium in the photocatalysts for degradation of trace $CHCl_3$ in drinking water.

| | Shell | Bond distance (Å) | Coordination number | Debye–Waller factor (Å²) |
|---|---|---|---|---|
| Ti-MCM-41 | Ti—$O_{eq}$ | 1.75 | 0.9 | 0.0058 |
| | Ti—$O_{ax}$ | 1.99 | 2.6 | 0.0029 |
| | Ti—(O)—Si | 3.13 | 2.9 | 0.0103 |
| $TiO_2$–$SiO_2$ | Ti—$O_{eq}$ | 1.77 | 1.9 | 0.0023 |
| | Ti—$O_{ax}$ | 2.32 | 2.5 | 0.0030 |
| | Ti—(O)—Si | 3.31 | 1.1 | 0.0027 |
| Nano $TiO_2$ | Ti—$O_{eq}$ | 1.92 | 1.5 | 0.0004 |
| | Ti—$O_{ax}$ | 2.03 | 3.1 | 0.0045 |
| | Ti—(O)—Ti | 3.03 | 3.5 | 0.0049 |
| $TiO_2$/SBA-15 | Ti—$O_{eq}$ | 1.90 | 2.0 | 0.0038 |
| | Ti—$O_{ax}$ | 1.99 | 3.3 | 0.0044 |
| | Ti—(O)—Ti | 3.03 | 2.1 | 0.0043 |

support interaction related to its relatively low CN. It seems that the $TiO_2$–$SiO_2$ contains sub-nano $TiO_2$ (supported on the $SiO_2$) that is not observed by XRD, which may behave like a $TiO_2$ cluster. The Ti—O—Si species are, in contrast, not found in the $TiO_2$/SBA-15. It seems that the $TiO_2$ nanoparticles may be formed in the hexagonally ordered mesoporous channels (an opening of 5.7 nm) of the SBA-15. Note that the averaged diameter of the $TiO_2$ nanoparticles in the SBA-15 is approximately 4.6 nm (see Table 2).

Photocatalytic degradation of trace $CHCl_3$ (500 p.p.b. in drinking water) by the nano, cluster and atomic dispersed $TiO_2$ photocatalysts under UV–vis radiation (250–800 nm) is shown in Fig. 4. An enhanced photocatalytic degradation of trace $CHCl_3$ by the Ti-MCM-41 is observed. After a 4 h UV–vis radiation, accumulated 28.8 p.p.m. $CHCl_3$ $gTiO_2^{-1}$ are photocatalytically degraded by Ti-MCM-41. The nano $TiO_2$ shows relatively low activity for photocatalytic degradation of
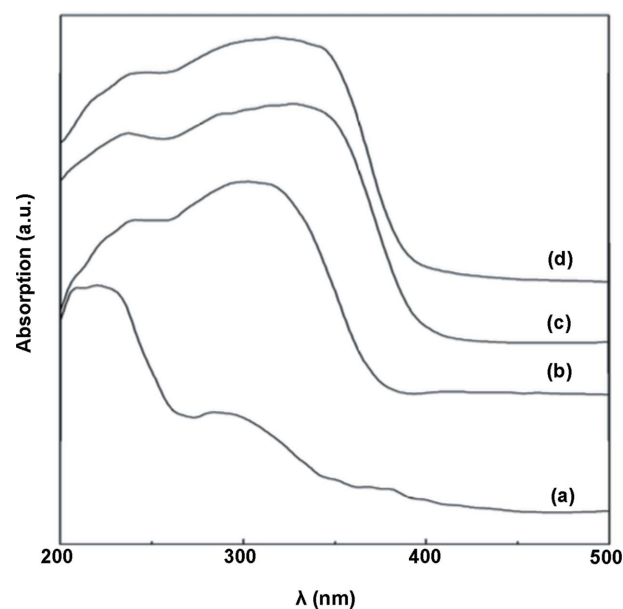


**Figure 1**
XRD patterns of (*a*) Ti-MCM-41, (*b*) $TiO_2$–$SiO_2$, (*c*) $TiO_2$/SBA-15 and (*d*) nano $TiO_2$.



**Figure 2**
DR UV–vis spectra of (*a*) Ti-MCM-41, (*b*) $TiO_2$–$SiO_2$, (*c*) nano $TiO_2$ and (*d*) $TiO_2$/SBA-15.

**Table 2**
Characterization and reactivity of the photocatalysts for degradation of trace $CHCl_3$ in drinking water.

$TiO_2$ chemical structure was determined by XRD. Crystalline size was calculated using the Scherrer equation. Band-gap absorption edge was determined by DR UV–vis. Photocatalytic degradation of $CHCl_3$ was determined in a total UV–vis reflectance system under UV–vis irradiation for 4 h [initial $CHCl_3$ concentration = 500 p.p.b. (in $H_2O$)]. Ti species were determined by XANES [$A_1$: $TiO_4$; $A_2$: $(Ti\!\!=\!\!O)O_4$; $A_3$: $TiO_6$]. Fractions of the Ti species (*i.e.* $A_1$, $A_2$ and $A_3$) related to the photocatalytic degradation of $CHCl_3$ determined by the linear regression analysis are well fitted for $A_2$ ($R^2 > 0.9$) while the $R^2$ values for $A_1$ and $A_3$ are 0.37 and 0.64, respectively.

| Photocatalyst | $TiO_2$ chemical structure | Crystalline size (nm) | Band-gap absorption edge (eV) | Photocatalytic degradation of $CHCl_3$ (p.p.m. $gTiO_2^{-1}\ h^{-1}$) | Ti species (%) | | |
|---|---|---|---|---|---|---|---|
| | | | | | $A_1$ | $A_2$ | $A_3$ |
| Ti-MCM-41 | Amorphous | – | 3.42 | 7.2 | 7 | 49 | 44 |
| $TiO_2$–$SiO_2$ | Amorphous | – | 3.38 | 0.9 | 25 | 33 | 42 |
| Nano $TiO_2$ | Anatase | 8.5 | 3.25 | 0.7 | 22 | 32 | 46 |
| $TiO_2$/SBA-15 | Anatase | 4.6 | 3.30 | 5.6 | 19 | 40 | 41 |

$CHCl_3$ when compared with the Ti-MCM-41. Note that the $TiO_2$–$SiO_2$ containing $TiO_2$ clusters also shows much less activity for the photocatalytic degradation than the $TiO_2$/SBA-15 that has larger $TiO_2$ nanoparticles (an average size of 4.6 nm). It appears that the reactivity with respect to photocatalytic degradation of trace $CHCl_3$ in drinking water may not be related to the crystalline phase, band-gap absorption edge or particle size of the $TiO_2$-based photocatalysts.

To reveal the key factor that influences the photocatalytic degradation reactivity of the $TiO_2$-based photocatalysts, Table 2 summarizes the characterization of the $TiO_2$-based photocatalysts, the related photocatalytic degradation reactivity and the photoactive sites involved. It seems that the photocatalysts, *i.e.* Ti-MCM-41 and $TiO_2$/SBA-15, possessing meso-pore channel systems have greater photocatalytic degradation conversions than the other ones that have nano and cluster $TiO_2$ on $SiO_2$. Apparently, the mesopores in the MCM-41 and SBA-15 have a large enough pore opening for free diffusion of small $CHCl_3$ molecules to the $TiO_2$ photoactive sites. Thus, there may exist other factors such as different loadings of $TiO_2$ and hardness or toxic ions in real drinking water that may also disturb the photocatalysis.

In Fig. 5, $A_1$ (4969 eV), $A_2$ (4971 eV) and $A_3$ (4972 eV) sites can be resolved in the pre-edge XANES spectra [between the absorption threshold (4966 eV) and jump (4984 eV)] of the photocatalysts. The $A_1$, $A_2$ and $A_3$ species in $TiO_2$ may be attributed to four- ($TiO_4$), five- [$(Ti\!\!=\!\!O)O_4$] and six- ($TiO_6$) coordinated Ti species, respectively (Hsiung *et al.*, 2006*a*, 2008). The B and C features (at 4974 and 4980 eV, respectively) are due to the interactions of the central Ti 4*p* orbitals hybridized with the near Ti or O atoms. The Ti *K* post-edge at 4980–5020 eV can be assigned to 3*s*-to-*np* dipole-allowed transitions. The insertion of Ti atoms into the $SiO_2$ matrix may cause dis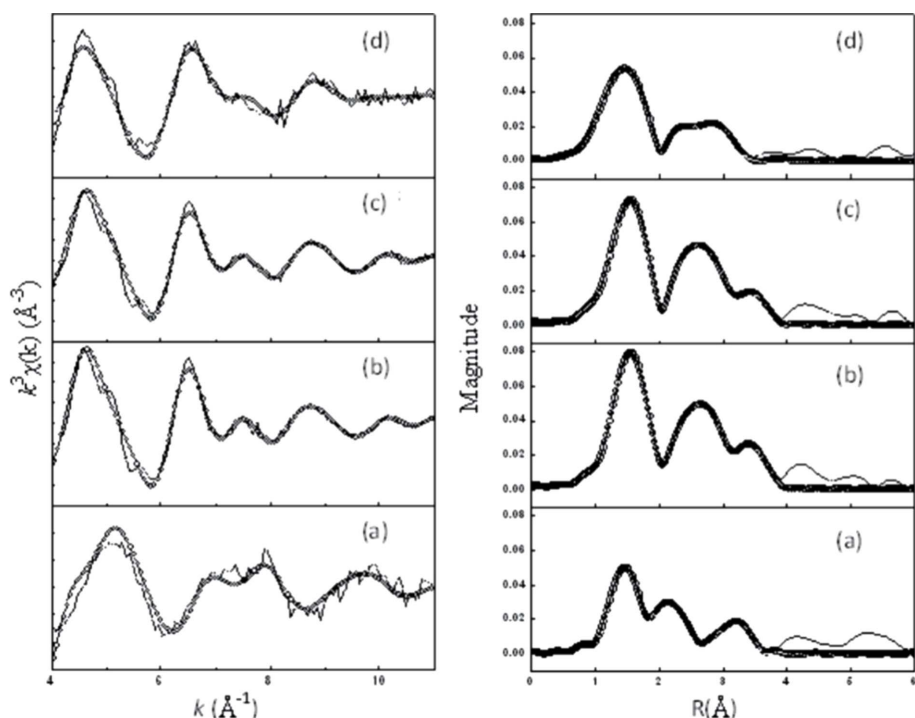tortion of the Ti–O octahedron structure. It is worth noting that the broadened white line absorption (4987 eV) for Ti-MCM-41 and $TiO_2$–$SiO_2$ is observed, suggesting the existence of highly dispersed Ti atoms in the $SiO_2$ matrix.

The Ti species ($A_1$, $A_2$ and $A_3$) in the photocatalysts were distinguished (in the XANES spectra). As shown in Table 2, the well dispersed Ti in Ti-MCM-41 has a much better performance for photocatalytic degradation of trace $CHCl_3$ in drinking water. The $A_2$ Ti species (fivefold-coordinated $Ti^{IV}$) possesses a square-pyramid structure, consisting of a double bond (Ti$=$O) and four Ti—O bonds, which is predominant generally on the surfaces of the very small (<10 nm) $TiO_2$ nanoparticles. Fractions of the Ti active species related to the photocatalytic degradation of $CHCl_3$ determined by the linear regression analysis are well fitted ($R^2 > 0.9$) while the $R^2$ values for $A_1$ and A3 are 0.37 and 0.64, respectively. The $A_2$ Ti species make a major contribution
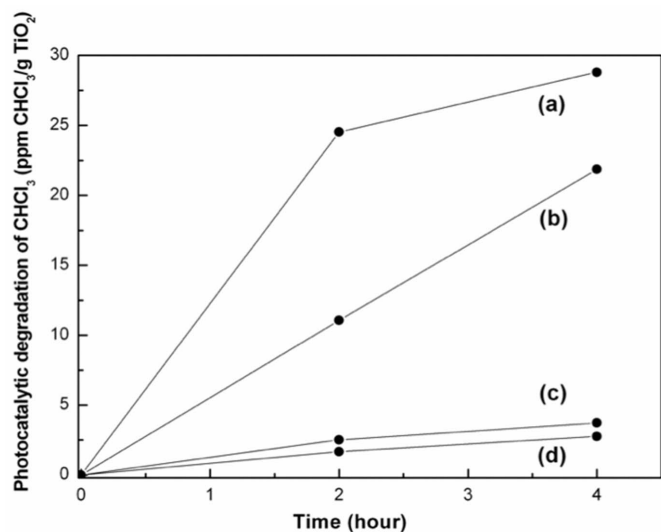


**Figure 3**
Ti *K*-edge XANES spectra of (*a*) $TiO_2$–$SiO_2$, (*b*) nano $TiO_2$, (*c*) $TiO_2$/SBA-15 and (*d*) Ti-MCM-41.

**Figure 4**
Time dependence for photocatalytic degradation of trace $CHCl_3$ in $H_2O$ effected by (*a*) Ti-MCM-41, (*b*) $TiO_2$/SBA-15, (*c*) $TiO_2$–$SiO_2$ and (*d*) nano $TiO_2$.

(75% approximately) to the photocatalytic degradation of trace $CHCl_3$ in $H_2O$. Note that about 95% of the photocatalytic conversion (7.2 p.p.m. $CHCl_3$ $gTiO_2^{-1}$ $h^{-1}$) is associated with the $A_2$ Ti active species in Ti-MCM-41.

## 4. Conclusions

The $A_1$ ($TiO_4$), $A_2$ [(Ti=O)$O_4$] and $A_3$ ($TiO_6$) Ti species in $TiO_2$ were observed and distinguished by component fitted pre-edge XANES spectra of the nano $TiO_2$ ($TiO_2$/SBA-15), $TiO_2$ cluster ($TiO_2$-$SiO_2$) and highly atomic dispersed Ti (Ti-MCM-41) photocatalysts. It appears that the photocatalytic degradation of trace $CHCl_3$ in drinking water may not be related to the crystalline phase, band-gap absorption edge or the particle size of the $TiO_2$-based photocatalysts. Nevertheless, the $A_2$ Ti species in the $TiO_2$-based photocatalysts may make a major contribution (75% approximately) to the overall photocatalytic performance. In the photocatalytic degradation of trace $CHCl_3$, for example, the higher $A_2$ Ti species in the atomic dispersed Ti (Ti-MCM-41) may account for 95% of the accumulated photocatalytic conversion. This work reveals that the $A_2$ Ti species of a $TiO_2$-based photocatalyst are associated significantly with its photocatalytic reactivity, especially in photocatalytic degradation of $CHCl_3$.
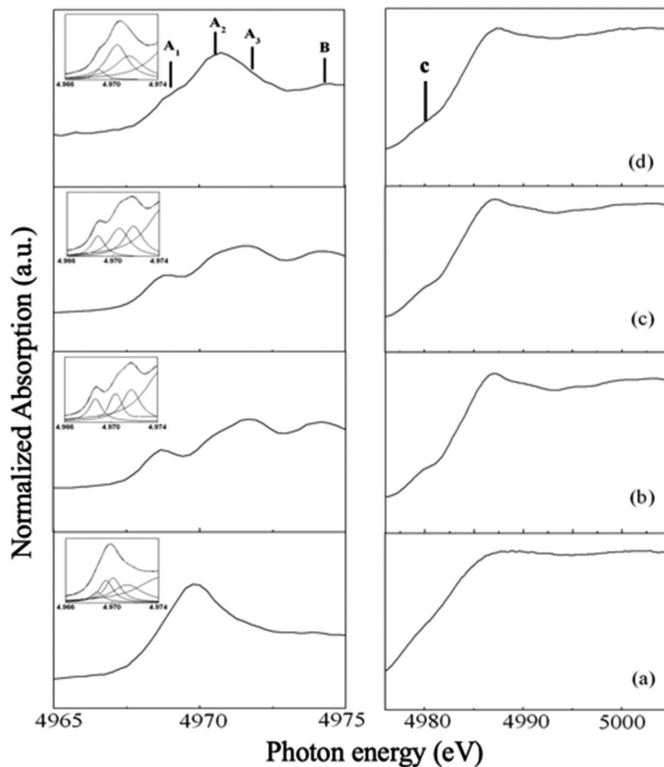
**Figure 5**
Ti *K*-edge XANES spectra of (*a*) $TiO_2$–$SiO_2$, (*b*) nano $TiO_2$, (*c*) $TiO_2$/SBA-15 and (*d*) Ti-MCM-41.

## References

Abou-Gamra, Z. M. & Ahmed, M. A. (2015). *Adv. Chem. Eng. Sci.* **05**, 373–388.

Beck, C., Mallat, T., Bürgi, T. & Baiker, A. (2001). *J. Catal.* **204**, 428–439.

Boorman, G. A. (1999). *Environ. Health Perspect.* **107** (Suppl. 1), 207–217.

Cai, Z., Dwivedi, A. D., Lee, W.., Zhao, X., Liu, W., Sillanpää, M., Zhao, D., Huang, C. & Fu, J. (2018). *Environ. Sci.: Nano*, **5**, 27–47.

Chen, F., Huang, H., Guo, L., Zhang, Y. & Ma, T. (2019). *Angew. Chem. Int. Ed.* **58**, 10061–10073.

Chien, Y. C., Wang, H. P. & Yang, Y. W. (2001). *Environ. Sci. Technol.* **35**, 3259–3262.

Chiu, Y. M., Huang, C. H., Chang, F. C., Kang, H. Y. & Wang, H. P. (2011). *Sustain. Environ. Res.* **21**, 279–282.

Diaz-Angulo, J., Gomez-Bonilla, I., Jimenez-Tohapanta, C., Mueses, M., Pinzon, M. & Machuca-Martinez, F. (2019). *Photochem. Photobiol. Sci.* **18**, 897–904.

El Mragui, A., Zegaoui, O. & Daou, I. (2019). *Mater. Today Proc.* **13**, 857–865.

Guo, J., Liang, J., Yuan, X., Jiang, L., Zeng, G., Yu, H. & Zhang, J. (2018). *Chem. Eng. J.* **352**, 782–802.

Hsiung, T. L., Wang, H. P. & Lin, S. & H. P. (2008). *J. Phys. Chem. Solids*, **69**, 383–385. .

Hsiung, T. L., Wang, H. P., Lu, Y. M. & Hsiao, M. C. (2006a). *Radiat. Phys. Chem.* **75**, 2054–2057.

Hsiung, T. L., Wang, H. P. & Wang, H. C. (2006b). *Radiat. Phys. Chem.* **75**, 2042–2045.

Hsiung, T.-L., Wei, L.-W., Huang, H.-L., Tuan, Y.-J. & Wang, H. P. (2021). *J. Synchrotron Rad.* **28**, 849–853.

Huang, Y. J., Wang, H. P. & Lee, J. F. (2003). *Appl. Catal. Environ.* **40**, 111–118.

Kang, H. Y. & Wang, H. P. (2013). *Environ. Sci. Technol.* **47**, 7380–7387.

Liao, C. Y., Wang, S. T., Chang, F. C., Wang, H. P. & Lin, H. P. (2014). *J. Phys. Chem. Solids*, **75**, 38–41.

Lin, L., Wang, K., Yang, K., Chen, X., Fu, X. & Dai, W. (2017). *Appl. Catal. Environ.* **204**, 440–455.

Lin, T. F. & Hoang, S. W. (2000). *Sci. Total Environ.* **246**, 41–49.

Liu, S. H., Huang, Y. J., Lin, K. S. & Hsiao, M. C. (2003). *Energy Sources*, **25**, 591–596.

Muñoz-Batista, M. J., Kubacka, A. & Fernández-García, M. (2014). *ACS Catal.* **4**, 4277–4288.

Pan, Y., Li, H., Zhang, X. & Li, A. (2016). *Trends Environ. Anal. Chem.* **12**, 23–30.

Sillanpää, M., Ncibi, M. C. & Matilainen, A. J. (2018). *J. Environ. Manage.* **208**, 56–76.

Wang, Z., Peng, X., Huang, C., Chen, X., Dai, W. & Fu, X. (2017). *Appl. Catal. Environ.* **219**, 379–390.

Xie, M. Y., Su, K. Y., Peng, X. Y., Wu, R. J., Chavali, M. & Chang, W. C. (2017). *J. Taiwan Inst. Chem. Eng.* **70**, 161–167.

Xu, C., Ravi Anusuyadevi, P., Aymonier, C., Luque, R. & Marre, S. (2019). *Chem. Soc. Rev.* **48**, 3868–3902.

Yang, C., Dong, W., Cui, G., Zhao, Y., Shi, X., Xia, X., Tang, B. & Wang, W. (2017). *Electrochim. Acta*, **247**, 486–495.

Yang, T. C., Chang, F. C., Wang, H. P., Wei, Y. L. & Jou, C. J. (2014). *Mar. Pollut. Bull.* **85**, 696–699.